Finite Element Analysis of Pulsed Laser Bending: The Effect of Melting and Solidification

X. Richard Zhang

Xianfan Xu[1]
e-mail: xxu@ecn.purdue.edu

School of Mechanical Engineering,
Purdue University,
West Lafayette, IN 47907-1288

This work developes a finite element model to compute thermal and thermomechanical phenomena during pulsed laser induced melting and solidification. The essential elements of the model are handling of stress and strain release during melting and their retrieval during solidification, and the use of a second reference temperature, which is the melting point of the target material for computing the thermal stress of the resolidified material. This finite element model is used to simulate a pulsed laser bending process, during which the curvature of a thin stainless steel plate is altered by laser pulses. The bending angle and the distribution of stress and strain are obtained and compared with those when melting does not occur. It is found that the bending angle increases continulously as the laser energy is increased over the melting threshold value. [DOI: 10.1115/1.1753268]

1 Introduction

Laser bending (or laser forming) is a non-contact technique capable of achieving very high precision. The schematic of a laser bending process is illustrated in Fig. 1. A target is irradiated by a focused laser beam passing across the target surface. Heating and cooling cause plastic deformation in the laser-heated area, thus change the curvature of the target permanently. The mechanism of laser bending has been explained by the thermo-elasto-plastic theory, [1–3]. Three laser bending mechanisms, i.e., the temperature gradient mechanism, the buckling mechanism, and the upsetting mechanism have been discussed in the literature, [4,5]. For the temperature gradient mechanism, a sharp temperature gradient is generated by laser irradiation and the residual compressive strain causes permanent bending deformation toward the direction of the incoming laser beam. Most of the pulsed laser bending processes are attributed to the temperature gradient mechanism since the short pulse heating duration induces a very sharp temperature gradient near the target surface.

Using a pulsed laser for bending is of particular interest in the micro-electronics industry, where high precision bending, curvature adjustment, and alignment are often required. Chen et al. [6] achieved bending precision on the order of sub-microradian on stainless steel and ceramics targets, which is higher than any other bending techniques. The relations between the bending angle and laser processing parameters were studied with the use of a two-dimensional finite element method, [7]. In that study, the laser energy was controlled so that no melting and solidification happened during the bending process. However, in some laser bending processes where larger bending angles are needed, the laser energy used could be high enough to cause melting, [8].

The finite element method is a general and powerful tool for investigating the complex thermal and thermomechanical problems involved in laser bending, [9–12]. When an unconstrained material melts, its stress and strain will be completely released, and then begin to retrieve when solidification starts. In this respect, the main challenge of simulations is the handling of the stress and strain release and retrieval during melting and solidification. The stress release is usually approximated by specifying the temperature dependent material properties, for example, decreasing Young modulus and yield strength significantly near the melting point, [9–12]. On the other hand, the strain release is hardly being considered due to the difficulty involved in the numerical simulation.

In this paper, a finite element model for simulating pulsed laser bending involving melting and solidification is developed using the uncoupled thermal and thermomechanical theory. It is assumed that the pulsed laser beam is uniform across the width of the specimen (the *x*-direction in Fig. 1). Thus, a two-dimensional thermal-stress model can be applied, which greatly reduces the computational time. In order to release and retrieve the stress and strain during melting and solidification, the element removal and reactivation method is applied to each melted element. In addition, in order to compute the stress of the solidified element correctly, a second reference temperature for the thermal stress calculation is used. The bending angle, residual stress, and residual strain are obtained and compared with the results of pulsed laser bending without melting.

2 Simulation Procedure

In order to calculate laser bending, a thermal analysis and a stress and strain analysis are needed, which are considered as uncoupled since the heat dissipation due to plastic deformation is negligible compared with the heat provided by laser irradiation. In an uncoupled thermomechanical model, a transient temperature field is obtained first in the thermal analysis, and is then used as a thermal loading in the subsequent stress and strain analysis to obtain the transient stress, strain, and displacement distributions. The finite element code, ABAQUS (HKS, Inc., Pawtucket, RI) is used. As shown in Fig. 2, a dense mesh is generated around the laser path and then stretched away in the length and thickness directions (the *y* and *z*-directions). The domain size and laser parameters used in the simulations are given in Table 1. The same mesh is used for both the thermal and stress analyses. A total of 1200 elements are used in the mesh. Mesh tests are conducted by increasing the number of elements until the calculation result is independent of the mesh density.

2.1 Thermal Analysis. The thermal analysis is based on solving the two-dimensional heat conduction equation:

$$\rho\tilde{c}\frac{\partial T}{\partial t}=\nabla\cdot(k\nabla T)+\dot{Q}_{ab} \tag{1}$$

[1]To whom correspondence should be addressed.

Contributed by the Applied Mechanics Division of THE AMERICAN SOCIETY OF MECHANICAL ENGINEERS for publication in the ASME JOURNAL OF APPLIED MECHANICS. Manuscript received by the ASME Applied Mechanics Division, Aug. 29, 2001; final revision, June 30, 2003. Associate Editor: B. M. Moran. Discussion on the paper should be addressed to the Editor, Prof. Robert M. McMeeking, Journal of Applied Mechanics, Department of Mechanical and Environmental Engineering University of California–Santa Barbara, Santa Barbara, CA 93106-5070, and will be accepted until four months after final publication of the paper itself in the ASME JOURNAL OF APPLIED MECHANICS.

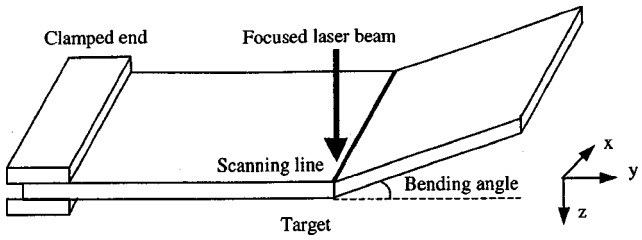

Fig. 1 Schematic of the laser bending process

where k is the thermal conductivity, ρ is the density of the stainless steel, $\tilde{c}$ is the derivative of the enthalpy with respect to temperature, and $\dot{Q}_{ab}$ is the volumetric heat source term resulted from irradiation of a laser pulse. The temperature-dependent properties of stainless steel 301, [13], are used in the calculation.

The parameter $\tilde{c}$ is equal to the specific heat c_p in solid and liquid regions. When an impure metal, like stainless steel, is heated from a solid state, it begins to melt at the solidus temperature T_s and melts completely at the liquidus temperature T_l. In the mushy zone, i.e., the region where the temperature is between T_s and T_l, $\tilde{c}$ is defined by

$$\tilde{c}=c_p+\frac{L}{T_l-T_s} \tag{2}$$

where L is the latent heat. Values of T_s, T_l, and L of stainless steel 301 are listed in Table 2, [13]. By using $\tilde{c}$, the effective specific heat, the phase change problem can be solved within a single domain. Solid and liquid material are treated as one continuous region and the phase boundary does not need to be calculated explicitly, [10].

The laser intensity is uniform in the x-direction and has a Gaussian distribution in the y-direction, expressed as

$$I_s(y,t)=I_0(t)e^{-8y^2/w^2} \tag{3}$$

where $I_0(t)$ is the time-dependent laser intensity at the center of the laser beam and w is the laser beam width at the target surface. The temporal profile of the laser intensity is treated as increasing linearly from zero to the maximum at 60 ns, then decreasing linearly to zero at the end of the pulse at 120 ns. Therefore, the volumetric heat source $\dot{Q}_{ab}$ in Eq. (1) can be expressed as

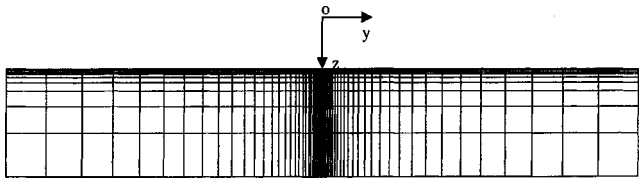

Fig. 2 Computational mesh

Table 1 Domain size and pulsed laser parameters

Specimen length (y)	600 μm
Specimen thickness (z)	100 μm
Laser wavelength	1.064 μm
Laser pulse full width	120 ns
Laser pulse energy	200–300 μJ
Laser line width	30 μm
Laser line length	1.3 mm

Table 2 Thermal properties of stainless steel 301

Solidus temperature, T_s	1673 K
Liquidus temperature, T_l	1693 K
Latent heat, L	265 J/g

$$\dot{Q}_{ab}=(1-R_f)\alpha I_0(t)e^{-8y^2/w^2}e^{-\alpha z} \tag{4}$$

where R_f is the optical reflectivity measured to be 0.66 for the stainless steel specimens. α is the absorption coefficient given by $\alpha=4\pi\kappa/\lambda$. The imaginary part of the refractive index κ of stainless steel 301 at the laser wavelength 1.064 μm is unknown, and $\kappa=4.5$ of iron is used. The initial condition is that the whole specimen is at the room temperature (300 K). Since the left and right boundaries as well as the bottom surface are far away from the laser irradiated area, the boundary conditions at these boundaries are prescribed as the room temperature. Convection and radiation with the surrounding are neglected.

Analyses are carried out with the laser pulse energy of 260 μJ, 270 μJ, 280 μJ, and 300 μJ, respectively. The peak temperature obtained by a 270 μJ pulse is 1703 K, higher than the liquidus temperature T_l (1693 K). For comparison, thermal analyses of three cases without melting are also performed; the laser pulse energies are 200 μJ, 230 μJ, and 250 μJ, respectively. The peak temperature obtained by a 250 μJ pulse is 1649 K, lower than the solidus temperature T_s (1673 K).

2.2 Stress and Strain Analyses. In the stress and strain analysis, the material is assumed to be linearly elastic-perfectly plastic. The Von Mises yield criterion is used to model the onset of plasticity. The left edge is completely constrained, and all other boundaries are force-free. Eight-node biquadratic plane-strain elements are employed.

As in the thermal analysis, the temperature dependent material properties are used, [13]. Poisson's ratio of stainless steel AISI 304, [14], is used. Considering the incompressibility in the liquid phase, the Poisson ratio of 0.4999 is used when the temperature is higher than T_s. The strain rate enhancement effect is neglected since temperature dependent data are unavailable. Sensitivity of unknown material properties on the computational results has been discussed by Chen et al. [7].

2.3 The Method of Element Removal and Reactivation In order to model the phenomena of melting and solidification, the element removal and reactivation method, [15], is applied. An element will be excluded from the stress and strain analysis when its temperature is higher than T_s, i.e., the element is removed from the domain after being melted and its stress and strain are released to zero. During cooling, the removed elements are reactivated in the calculation when their temperatures are lower than T_s and the stress and strain start to retrieve.

For the elements starting to solidify, the initial temperature for the thermal stress calculation T_i is replaced with a new initial temperature equal to the temperature at the moment when it is reactivated, i.e., T_s. This procedure is carried out for each element experiencing melting and solidification with the aid of the temperature history data obtained from the thermal analysis.

The reason for using a new initial temperature for a reactivated element is explained as follows. As mentioned before, the thermal stain of an unconstrained element is totally released after it melts. During solidification, the thermal strain will change gradually only if T_s is used as the initial temperature. Otherwise, if the room temperature T_i is still used as the initial temperature, the thermal strain will experience a sharp jump from zero to a high value, which is physically incorrect. Therefore, two initial temperatures should be used for each element involving melting and solidification.

The element removal and reactivation would not affect the thermal analysis since the thermal and the stress analysis are not coupled, and the thermal analysis is performed before the stress analysis. The forces in the element reaching the melting point are reduced to zero gradually before the element is removed, which is determined by the temperature-dependent stress-strain relations. Therefore, there is no sudden change of stress in elements involved in phase change. On the other hand, when the element is reactivated with zero stress, it exerts no nodal forces on the sur-

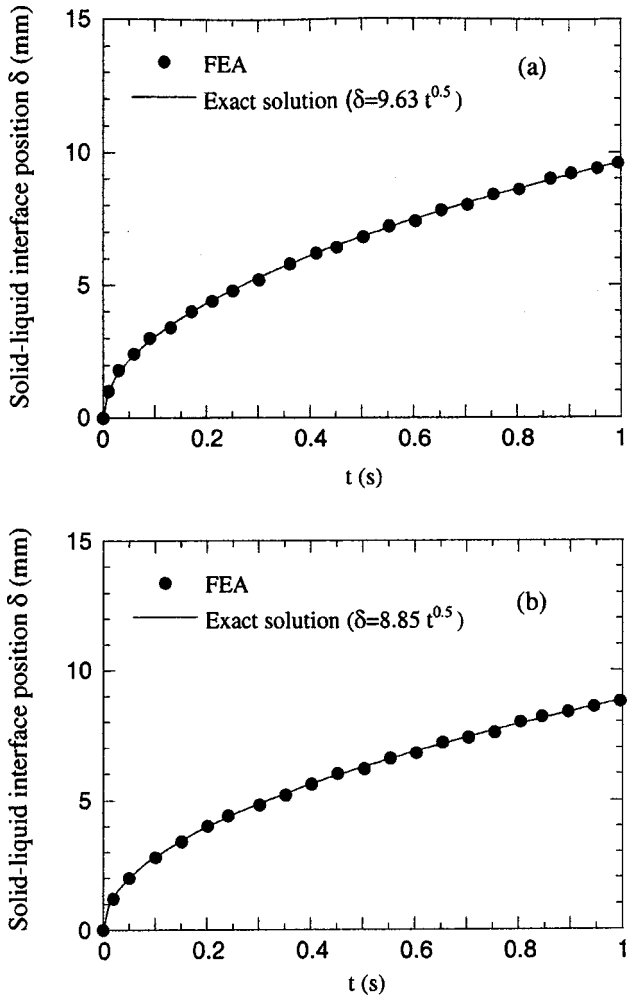

Fig. 3 Comparison between the results of FEA and an exact solution for (*a*) solidification, (*b*) melting

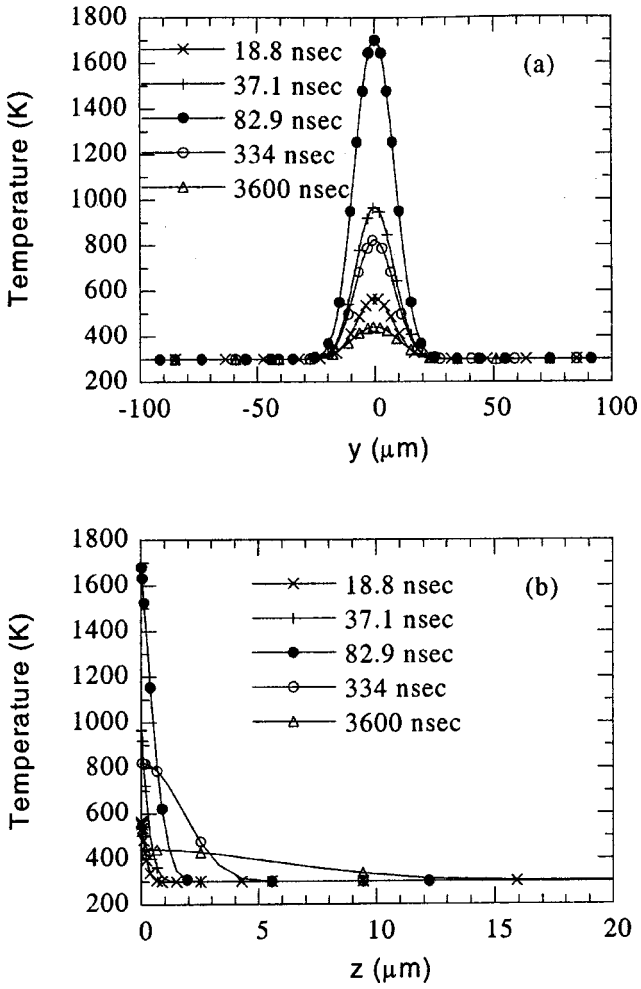

Fig. 4 Temperature distributions at different moments ($E = 270\ \mu J$) (*a*) along the *y*-direction on the top surface, (*b*) along the *z*-direction (at $y = 0$)

rounding elements. Thus the element removal and reactivation do not have any adverse effect on the thermal and stress calculation.

Based on the above description, the stress and strain for the elements involved in phase change are computed by the method of element removal and reactivation and the use of a new initial temperature at T_s to calculate the stress/strain of the solidified elements. During the calculation, element removal and reactivation are tracked for each element since each melted element begins to melt and solidify at different times. Hence, the computation is intensive even for the two-dimensional problem considered in this work.

3 Results and Discussion

Calculations are first conducted to verify the finite element analysis of melting and solidification. Results of finite element analysis are compared with exact solutions of solidification and melting problems given by Carslaw and Jaeger [16]. For the solidification case, the target is initially at the liquid state with a uniform temperature. At $t = 0$, the temperature at the surface ($x = 0$) is changed and held at a temperature lower than the melting point. Freezing thus starts and proceeds into the material. The position of the solid-liquid interface δ can be calculated with known material properties, and its expression is given in the insert of Fig. 3(*a*). Figure 3(*a*) shows the comparison of the results. It can be seen that the result of the finite element analysis matches exactly with the analytical solution. Similarly, results of the melting case are also compared. In this case, the target is initially at the solid state at the melting point. At $t = 0$, the surface temperature is increased to and kept at a constant temperature higher than the melting point. Again, exact match between the finite element result and the analytical solution is obtained, as shown in Fig. 3(*b*).

The above calculations are the only ones relevant to the problem studied here which have analytical solutions. There are no analytical solutions for thermomechanical problems with solid/liquid phase change since these problems are highly nonlinear. The rest of this work is focused computing the laser bending problem involving melting and solidification. We first present detailed temperature and residual stress distributions induced by a laser pulse at a fixed energy (270 μJ). Then, the laser pulse energy is varied, and bending with and without melting is compared in terms of the thermal strain, plastic strain, total strain, and stress. The dependence of the bending angle on the laser energy is also presented.

3.1 Results of Laser Bending With a Pulse Energy of 270 μJ. The transient temperature distribution in the target in first calculated. Figure 4 shows temperature distributions along the *x* and *z*-directions at different times. It can be seen that the maximum temperature, T_{max}, is obtained at the pulse center and reaches its peak value of 1703 K at 82.9 ns, and then drops slowly to 446 K at 3.6 μs. It can be estimated that the heat affected zone (HAZ) is around 40 μm wide (the laser beam is 30 μm wide). Figure 4(*b*) is the temperature distribution along the *z*-direction,

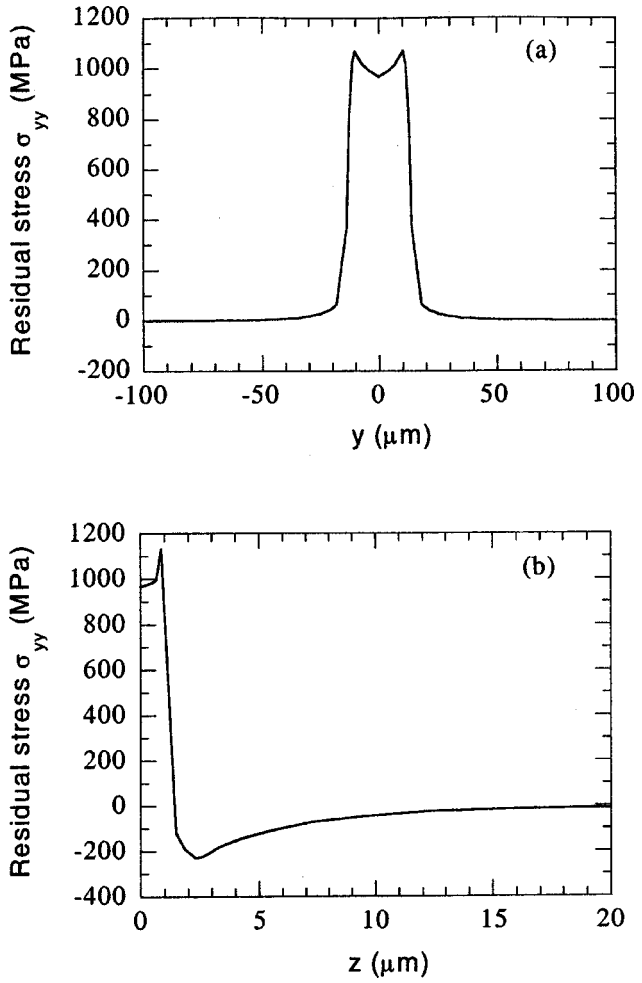

Fig. 5 Residual stress σ_{yy} distributions ($E=270\ \mu J$) (*a*) along the *y*-direction on the top surface, (*b*) along the *z*-direction (at $y=0$)

beginning from the upper surface of the target. It can be seen that the temperature gradient during heating period is higher than 500 K/μm.

Distributions of the transverse residual stress σ_{yy} along the *y* and *z*-directions are shown in Fig. 5. It can be seen from Fig. 5(*a*) that σ_{yy} is tensile, and has a value larger than 1.0 GPa. The stress-affected zone in the *y*-direction is about 30 μm. In the *z*-direction, σ_{yy} is more than 1.0 GPa within 1.0 μm from the surface. It becomes compressive at a depth of 1.5 μm from the surface. The maximum value of the compressive stress is about 250 MPa at $z=2.5\ \mu$m, and it gradually reduces to zero in the deeper region.

Figure 6 shows the deformation distribution along the *y*-direction. It can be seen that the permanent bending deformation is in the direction toward the incoming laser beam and the deflection is 42 nm at the free edge ($y=300\ \mu$m). There is a "Λ" shape surface deformation around $y=0\ \mu$m, the center of the laser beam. This is produced by thermal expansion along the negative *z*-direction because the surface is not constrained.

Detailed information about the thermal strain, the total strain, and the stress for the elements involved in melting and solidification and computed using the element removal and retrieval method is presented next, together with the case without melting for comparing their values.

3.2 Comparison Between Laser Bending With and Without Melting. Strain and stress histories during laser bending with melting (270 μJ) are compared with those without melting

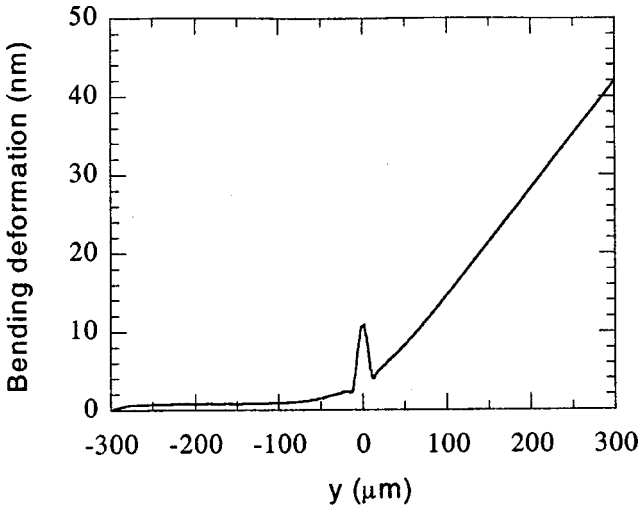

Fig. 6 Bending deformation along the *y*-direction ($E=270\ \mu J$)

(250 μJ). With the pulse laser energy of 270 μJ, the target begins to melt at about 70 ns and is completely solidified after 200 ns. Results of the center element on the top surface are compared.

Figure 7 shows histories of the thermal strain. For laser bending without melting, the thermal strain first increases as the temperature rises due to laser irradiation, and reaches a maximum value of 0.0228 at 82.03 ns. It then reduces to zero as the target cools to the room temperature. However, for bending involving melting, there are three periods in the thermal strain development: heating, melting and solidification, and cooling. The thermal strain reaches the peak value of 0.0232 at 69.52 ns. At this time, the corresponding average temperature of the element is 1673 K, which equals the solidus temperature. The element is excluded from the stress and strain analyses when it melts, which lasts for more than 28 ns. When it starts to solidify at 97.52 ns, the initial temperature of the element is replaced by the solidus temperature T_s, and then the thermal strain starts from zero to retrieve a negative value, which decreases continuously and reaches a residual value of -0.0229. The final thermal strain is very different from that of the nonmelting case because of the use of a second initial temperature.

Transverse plastic strains with and without melting are shown in Fig. 8. The compressive plastic strains are created during the

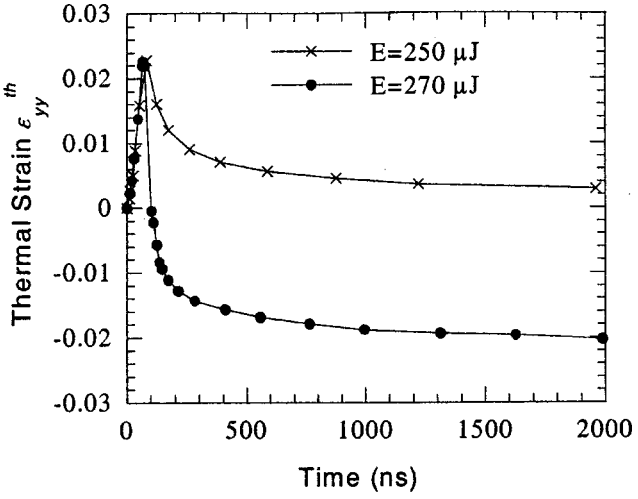

Fig. 7 Transient thermal strain at the center point on the top surface

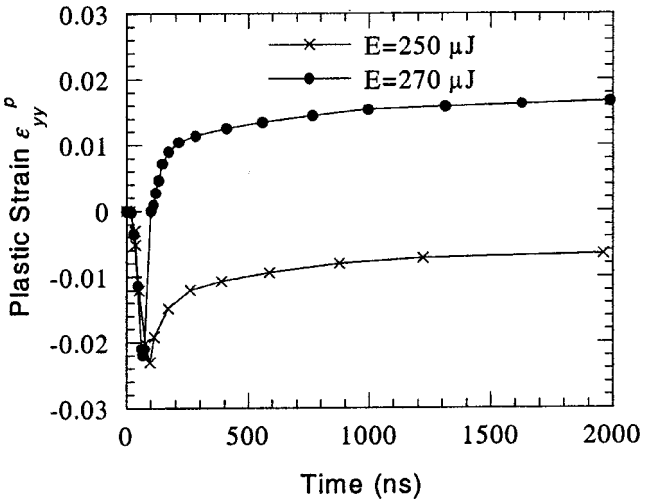

Fig. 8 Transient plastic strain at the center point on the top surface

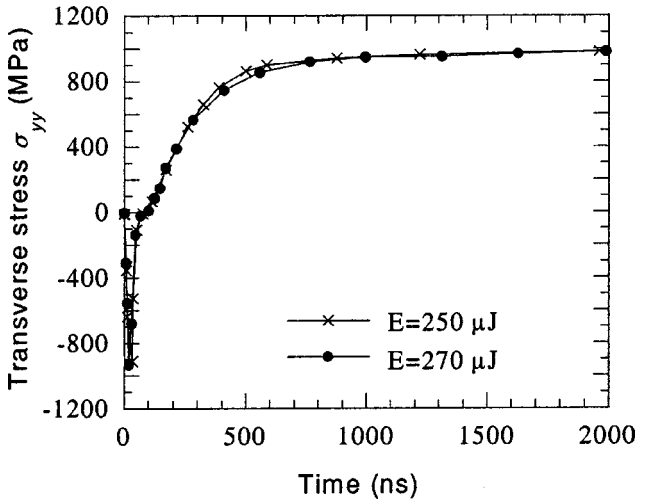

Fig. 10 Transient transverse stress σ_{yy} at the center point on the top surface

heating period since the thermal expansion of the heated area is constrained by the surrounding cooler materials. In the subsequent cooling period, the plastic strain decreases gradually, and is partially canceled with a residual value of −0.0047 for the case without melting. For bending involving melting, the compressive plastic strain is created during heating and it is released to zero during melting. This represents a significant difference between the two cases. Physically, the melted material can not support any strain due to the free surface while the material not melted can support a relatively large strain because of the surrounding cooler material, which is exactly what modeled here and shown in the results. After the melted element begins solidified, a tensile plastic strain develops, and a residual plastic strain of 0.0185 is obtained.

The history of the total transverse strain ε_{yy} up to 2000 ns is shown in Fig. 9. Despite the differences in the thermal and plastic strains, it can be seen that the total strains in both cases have a similar trend. The total strain increases and then decreases, and at about 100 ns it increases rapidly and reaches the maximum value at around 400 ns as the target bends away from the laser beam. After that, it decreases slowly and the residual value is about −0.0015 for bending without melting and −0.0017 for bending with melting (not shown in the figure). In both cases, the final bending angle is positive, meaning in the direction toward the laser beam.

Unlike strain, the overall trend of the stress development is not much affected by melting and solidification. As shown in Fig. 10, the development of the transverse stress follows a similar trend and a tensile residual stress of about 0.97 GPa is obtained in both cases. This is because the yield stress and the Young's modulus are reduced significantly at high temperature. Fort the case without melting, the stress is released to almost zero near the melting point, while the stress is reduced to zero for the case with melting.

Figure 11 shows the relation between the bending angle and the pulse energy. Bending angle increases almost linearly with the pulse energy. The dash line is the fitted line for laser bending without melting and is extracted to compare with the data with melting. There is no discontinuity or large change in the relation between the bending angle and the laser energy when the laser energy is increased across the melting threshold. This is in consistent with the results of total strain calculations since bending is

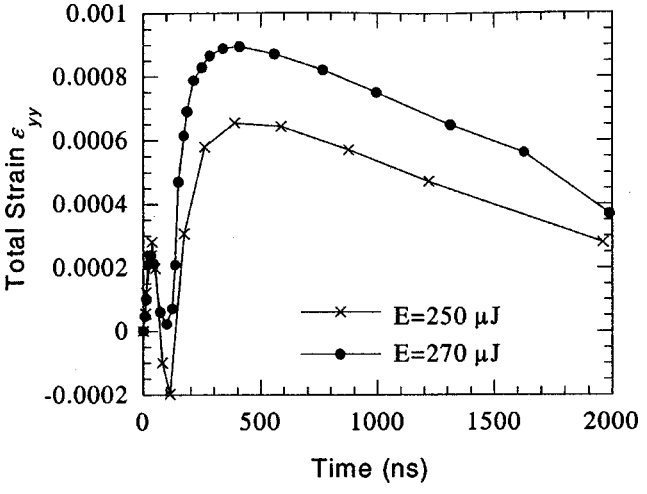

Fig. 9 Transient total strain ε_{yy} at the center point on the top surface

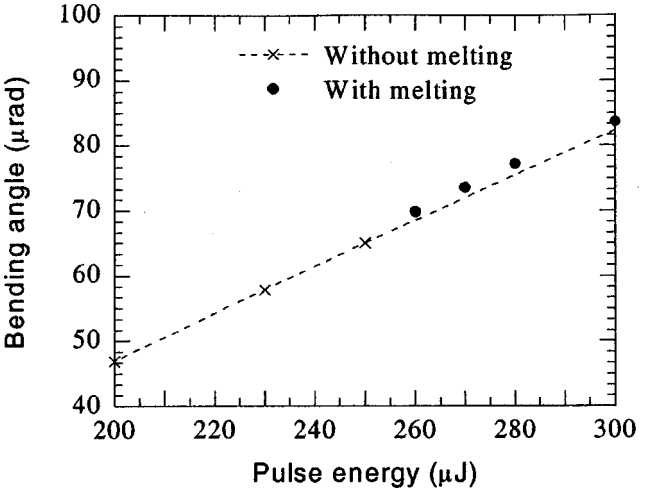

Fig. 11 Bending angle as a function of laser pulse energy

directly related to the total residual strain. As discussed previously, no large change of the total strain is found when the laser-energy is increased across the melting threshold.

4 Conclusion

A two-dimensional finite element model for calculating pulsed laser bending with melting and solidification is developed. The element removal and reactivation method is applied to each melted element to account for the stress and strain release in the melted material. A second initial temperature is necessary for the reactivated elements in order to compute the stress and strain development correctly. The bending angle and the residual stress and strain distribution of stainless steel irradiate by a laser pulse are obtained using this model. Results are also compared with those of laser bending without melting. No sudden change of the total residual strain, stress, and the bending angle is found when the laser energy is increased across the melting threshold.

Acknowledgment

Support of this work by the National Science Foundation (DMI-9908176) is gratefully acknowledged.

Nomenclature

E = laser pulse energy
I_0 = laser intensity at the center of the laser beam
I_s = laser flux
L = latent heat
$\dot{Q}_{ab}$ = volumetric heat source term induced by irradiation of a laser pulse
R_f = optical reflectivity
T = temperature
T_l = liquidus temperature
T_s = solidus temperature
$\tilde{c}$ = effective specific heat
c_p = specific heat
k = thermal conductivity
t = time
w = laser beam width
x, y, z = Cartesian coordinates
α = absorption coefficient
δ = position of solid-liquid interface
ε_{yy} = total strain along the y-direction
ε_{yy}^{p} = plastic strain along the y-direction
ε_{yy}^{th} = thermal strain along the y-direction
κ = imaginary part of the refractive index
λ = wavelength
ρ = density
σ_{yy} = stress along the y-direction

References

[1] Namba, Y., 1986, "Laser Forming in Space," *International Conference on Lasers*, C. P. Wang et al., eds., STS Press, Las Vegas, NV, pp. 403–407.
[2] Scully, K., 1987, "Laser Line Heating," J. Ship Prod., **3**, pp. 237–246.
[3] Arnet, H., and Vollertsen, F., 1995, "Extending Laser Bending for the Generation of Convex Shapes," Proc. Inst. Mech. Eng., **209**, pp. 433–442.
[4] Vollertsen, F., 1994, "Mechanisms and Models for Laser Forming," *Laser Assisted Net Shape Engineering, Proc. of the LANE*, M. Geiger et al., eds., Meisenbach, Bamburg, Germany, **1**, pp. 345–360.
[5] Geiger, M., and Vollertsen, F., 1993, "The Mechanisms of Laser Forming," Annals of the CIRP, **42**, pp. 301–304.
[6] Chen, G., Xu, X., Poon, C. C., and Tam, A. C., 1998, "Laser-Assisted Microscale Deformation of Stainless Steels and Ceramics," Opt. Eng., **37**, pp. 2837–2842.
[7] Chen, G., Xu, X., Poon, C. C., and Tam, A. C., 1999, "Experimental and Numerical Studies on Microscale Bending of Stainless Steel With Pulsed Laser," ASME J. Appl. Mech., **66**, pp. 772–779.
[8] Zhang, X., and Xu, X., 2001, "Fundamental and Applications of High Precision Laser Micro-Bending," IMECE, ASME, New York.
[9] Feng, Z., Zacharia, T., and David, S. A., 1997, "Thermal Stress Development in a Nickel Based Superalloy During Weldability Test," Weld. Res. Suppl., Nov., pp. 470–483.
[10] Lewis, R. W., and Ravindran, K., 1999, "Finite Element Simulation of Metal Casting," Int. J. Numer. Methods Eng., **47**, pp. 29–59.
[11] Taljat, B., Zacharia, T., and Wang, X., etc., 1998, "Numerical Analysis of Residual Stress Distribution in Tubes With Spiral Weld Cladding," Weld. Res. Suppl., Aug., pp. 328–335.
[12] Taljat, B., Radhakrishman, B., and Zacharia, T., 1998, "Numerical Analysis of GTA Welding Process With Emphasis on Post-Solidification Phase Transformation Effects on Residual Stresses," Mater. Sci. Eng., A, **246**, pp. 45–54.
[13] Maykuth, D. J., 1980, *Structural Alloys Handbook*, Metals and ceramics information center, Battelee Columbus Laboratories, Columbus, OH, **2**, pp. 1–61.
[14] Takeuti, Y., and Komori, S., 1979, "Thermal-Stress Problems in Industry 3: Temperature Dependency of Elastic Moduli for Several Metals at Temperatures From −196 to 1000°C," J. Therm. Stresses, **2**, pp. 233–250.
[15] *ABAQUS User's Manual*, Version 5.8, 1997, Hibbitt, Karlsson and Sorensen, Inc.
[16] Carslaw, H. S., and Jaeger, J. C., 1959, *Conduction of Heat in Solids*, 2nd Ed., Oxford University Press, Oxford, UK, Chap. XI, pp. 285–288.